Joint Hybrid 3D Beamforming Relying on Sensor-Based Training for Reconfigurable Intelligent Surface Aided TeraHertz-Based Multi-user Massive MIMO Systems

Xufang Wang, *Member, IEEE,* Zihuai Lin, *Senior Member, IEEE*, Feng Lin, *Member, IEEE,* and Lajos Hanzo, *Life Fellow*

***Abstract*— Terahertz (THz) systems have the benefit of high bandwidth and hence are capable of supporting ultra-high data rates, albeit at the cost of high pathloss. Hence they tend to harness high-gain beamforming. Therefore a joint hybrid 3D beamformer relying on sophisticated sensor-based beam training and channel estimation is proposed for *Reconfigurable Intelligent Surface* (RIS) aided THz Multi-user Massive *Multiple Input Multiple Output* (MIMO) systems. A novel joint subarray based THz base station (BS) architecture and the corresponding sub-RIS is proposed. The BS, RIS and receiver antenna arrays of the users are all *Uniform Planar Arrays* (UPAs). Moreover, the conditions of maintaining the orthogonality of the proposed joint architecture are derived in support of spatial multiplexing. The closed-form expressions of the near-field and far-field pathloss are also derived. The *Ultra-wideband* (UWB) sensors are integrated into the RIS and the user location information obtained by the UWB sensors is exploited for channel estimation. The optimal active and passive beamforming schemes are also derived. Moreover, *Precise Beamforming Algorithm* (PBA) for joint RIS phase shift and *user equipment* (UE) receiver beamforming is proposed, which further improves the beamforming accuracy by circumventing the performance limitations imposed by positioning errors. Our simulation results show that the proposed system significantly improves the spectral efficiency, despite its low complexity. Compared to the scheme operating without PBA, our proposed scheme increases the spectral efficiency on average by 10.41%, 10.17%, and 5.19% for the three farfield configurations, and by 5.05% and 3.95% for the two nearfield configurations, respectively. This makes our solution eminently suitable for delay-sensitive applications.**

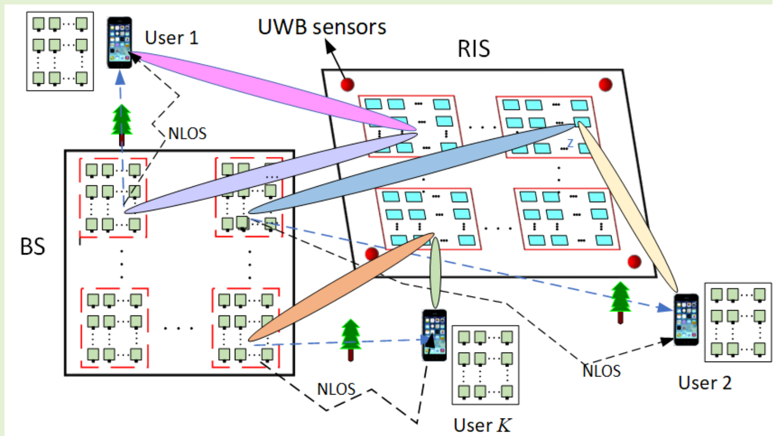

***Index Terms*— Joint hybrid 3D beamforming, TeraHertz, UWB sensors, beam-training, sub-RIS.**

I. Introduction

The data rate requirements of wireless communications have increased rapidly with the explosive growth of mobile devices and seamless multimedia applications. Hence, the bandwidth available in the sub-6 *Gigahertz* (GHz) and mmWave bands becomes tight, but as a remedy, the *Terahertz* (THz) range of (0.1-10 THz) may be explored for 6G development [1]. Given its short wavelength, a large number of antennas can be packed into a compact transceiver. Graphene based plasmonic massive MIMO nano-antenna arrays have been developed in [2] for the THz band, relying on beamforming based angular multiplexing [3]. However, traditional systems using a dedicated RF chain for each antenna are no longer practical due to the unacceptable hardware costs. In [4], a hybrid beamforming system associated with an array-of-subarray structure is proposed for THz communications,

This work was supported by the Fujian Provincial Department of Science, and Technology Project under Grant 2019J01267. L. Hanzo would like to acknowledge the financial support of the Engineering and Physical Sciences Research Council projects EP/P034284/1 and EP/P003990/1 (COALESCE) as well as of the European Research Council's Advanced Fellow Grant QuantCom (Grant No. 789028) *(Corresponding author: Lajos Hanzo.)*

Xufang Wang is with the Key Laboratory of Optoelectronic Science and Technology for Medicine of Ministry of Education, Fujian Normal University, Fuzhou, China (e-mail: fzwxf@fjnu.edu.cn).

Zihuai Lin is with the School of Electrical and Information Engineering, University of Sydney, Sydney, NSW 2006, Australia (e-mail: zihuai.lin@sydney.edu.au).

Feng Lin is with Kongtronics Institute of Science and Technology (XiaMen) Co., Ltd., Xia Men, China (e-mail: helloyou@189.cn).

Lajos Hanzo is with the University of Southampton, SO17 1BJ Southampton, U.K. (e-mail: lh@ecs.soton.ac.uk).

in which the number of RF chains is much smaller than the number of antennas.

In addition, although THz communication [5] [6] and sensing [7] have the advantage of increasing the bandwidth by orders of magnitude, it inherently suffers from limited coverage range due to the diffusion loss caused by high frequencies, the absorption of molecules in the atmospheric medium and the higher probability of *line-of-sight* (LOS) blockage [8]. A feasible way forward is to combine the massive MIMO transciever with a *reconfigurable intelligent surface* (RIS), whose phase shift can be controlled by a low-complexity programmable PIN diode [9] in support of 6G systems [10]. It can improve the propagation conditions by introducing controllable scattering to obtain beneficial beamforming gains and mitigate the interference [11]. This is achieved by increasing the freedom of transceiver design and network optimization by intelligently ameliorating the wireless propagation environments [12].

Despite the fact that the RIS optimization of most *Multiple Input Single Output* (MISO) systems can be directly transformed into quadratic programming under quadratic constraints, there is a paucity of literature on the design of RIS assisted MIMO systems [13], [14]. Hence, we conceive a Mulit-user massive MIMO-aided and RIS assisted THz system. Additionally, most of the open literature assumes that the channel state information (CSI) of the RIS is perfectly available [11] [15] [16] However, since all elements of the RIS are passive, it cannot send, receive or process any pilot signal for channel estimation. Moreover, a RIS usually contains hundreds of elements, so the dimension of the estimated channel is much higher than that of traditional systems, hence requiring an excessive pilot overhead. Therefore, traditional methods cannot be directly applied, and channel estimation is a key challenge [17], especially for RIS-aided THz multiuser massive MIMO systems. The phase shift opimization and passive beamforming in THz RISs also constitute challenges. Therefore, sophisticated schemes have been proposed for the channel estimation of RIS-aided MISO systems [8] [18] [19] [20], where the receiver is equipped with a single antenna. However, these schemes cannot be readily combined with the above-mentioned channel estimation schemes in massive MIMO systems. A cooperative beam training scheme is developed in [21] to facilitate the estimation of the concatenated twin-hop BS-RIS-UE channel. However, they assumed having no obstacles between the BS and users, which may not always be the case. In [22], the location information obtained by GPS is used to assist RIS systems, but the altitude error of GPS is quite high, about twice as high as that on the ground, rendering the system performance severely affected by the GPS errors. Moreover, GPS often fails in obstructed open areas or indoors. By comparison, UWB wireless positioning can reach centimeter level accuracy [23].

On the other hand, given its compelling benefits, *Integrated Sensing and Communication* (ISAC) [24] have attracted substantial research attention. In this context, a number of ISAC schemes have been proposed. For example, the co-existence and joint transmission for a MIMO *Radar-Communication* (RadCom) system is proposed in [25] subject to specific *Signal to Interference and Noise Ratio* (SINR) constraints. They also proposed a mmWave Massive MIMO ISAC system operating in the face of interference [24]. A new cooperative method was proposed in [26] for distributed target tracking relying on the fusion of OFDM-based radar and communication. However, traditional beam training methods are unsuitable for the extremely narrow pencil beams of THz waves. Minor misalignment in THz RIS passive beamforming with respect to the users will result in severely degraded system performance. To tackle the 3D beam training problem of RIS-aided THz multi-user massive MIMO networks, we will integrate UWB sensors into our system architecture and derive the optimal passive beamforming weights - which may contain estimation errors - as the initial input value of the algorithm. Thus the efficiency of the beam training algorithm can be substantially improved. The beam training optimization feedback may also beneficially support 3D sensor networks in the *Internet of Underwater Things* (IoUT) [27], and in *Space-Air-Ground Integrated Networks* (SAGIN) [28].

In this paper a novel joint hybrid 3D beamformer relying on a sensor-based beam training and channel estimation scheme is proposed for RIS assisted THz multi-user massvie MIMO systems. Explicitly, a novel joint architecture of subarray-based THz base stations (BS) and the corresponding sub-RISs is proposed. The RIS can be installed both on building walls, facades and even on *unmanned aerial vehicles* (UAV) for supporting 3D passive beamforming. We have also derived the conditions of spatial multiplexing for the proposed system architecture in RIS-aided THz networks, which has not been addressed before in the literature. The BS, RIS and the receiver antenna arrays are all UPAs. The UWB sensors are integrated into the RIS and the user location information obtained by UWB sensors is used for channel estimation and beamforming. The optimal active and passive beamforming are derived and a so-called *Precise Beamforming Algorithm* (PBA) is proposed, which is capable of improving the beamforming accuracy by eliminating the deleterious effects of positioning errors. Simulation results show that our proposed system can achieve significant improvement of the the spectral efficiency by the proposed beam training scheme.

Against the above backdrop, our main contributions are:

1) We propose a novel joint hybrid 3D beamforming–BS array-of-subarray and the corresponding sub-RIS architecture for RIS-aided THz multi-user massive MIMO systems. Furthermore, we have derived the conditions of orthogonality for the proposed architecture in support of spatial multiplexing;

2) We conceive a UWB sensor-based channel estimator for the proposed architecture. We have derived the optimal active and passive beamforming, and proposed the PBA concept based on user location information for joint RIS phase shift and *user equipment* (UE) receiver beamforming. Thus, the beamforming accuracy is improved and the system performance is no longer constrained by the positioning errors of the sensors, yet compared to other beam training schemes our proposed scheme has the lowest complexity and search time, rendering it eminently suitable for users having time-varying positions or delay-sensitive applications;

3) We have derived the closed-form expressions for both the

near-field and far-field path-loss of RIS-aided THz channels. Both the near-field and far-field scenarios demonstrate the efficiency of our proposed scheme.

4) The performance of the proposed system will not be constrained by the number of users and there is almost no interference among multiple users. Since the operations of the users are carried out in parallel, the algorithmic complexity will not be affected by the number of users. Additionally, the BS subarrays and sub-RISs of the proposed architecture can be flexibly or dynamically configured to meet the specific needs of users.

5) Our proposed 3D beamforming architecture relying on UPAs is eminently suitable for a range of emerging RIS aided THz applications, such as the integration of terrestrial links, UAVs, and satellite systems, since THz transceivers can be fabricated as an array-of-subarrays of constructed graphene-based plasmonic nano-antennas [2] and THz RISs can also be fabricated based on metal/graphene hybrid materials [29]. The provision of beamforming optimization feedback is also beneficial for sensor networks in 3D scenarios.

In Table I we boldly and explicitly contrasting the novelty of our paper to the state-of-the-art at a glance.

The remainder of the paper is organized as follows. In Section II, we describe both the system model, channel models and proposed architecture. In Section III, we explore the channel conditions to be satisfied for high-integrity spatial multiplexing in our proposed architecture. In Section IV, the closed-form expressions of the path-loss of the RIS-aided near-field and far-field beamforming channels are derived. In Section V, the proposed sensor based channel estimation and beam training scheme is presented. Our performance analysis is discussed in Section VI, followed by our simulation results in Section VII. Finally, we conclude in Section VIII.

Notation: Boldface lower case and upper case letters are used for column vectors and matrices, respectively. The superscripts $(\cdot)^*$, $(\cdot)^T$, $(\cdot)^H$, and $(\cdot)^{-1}$ stand for the conjugate, transpose, conjugate-transpose, and matrix inverse, respectively. The Euclidean norm, absolute value, Hadamard product are denoted by $||\cdot||$, $|\cdot|$ and $\odot$ respectively. In addition, $\mathbb{E}\{\cdot\}$ is the expectation operator. For a matrix $\mathbf{A}$, $[\mathbf{A}]_{mn}$ denotes its entry in the *m*-th row and *n*-th column, while for a vector $\mathbf{a}$, $[\mathbf{a}]_m$ denotes the *m*-th entry of it. Furthermore, j in $e^{j\theta}$ denotes the imaginary unit, while $\mathbf{I}$ is the identity matrix.

II. System Model, Channel Models and Proposed Architecture

In this section, we introduce the system model and the channel models of 3D hybrid beamforming designed for RIS-assisted THz MIMO systems, including the direct BS-to-user path and the BS-RIS-user path. It is worth mentioning that in the system model of the BS-RIS-user path, a novel joint hybrid 3D beamforming–BS array-of-subarray and the corresponding sub-RIS architecture is proposed for RIS-aided THz multi-user massive MIMO systems, which will be further detailed in the following sections.

The system model we adopted is shown in Fig. 1. The THz transceivers have array-of-subarrays of graphene-based plasmonic nano-antennas [2]. The BS transmitter (TX) having $L_B = M_t \times N_t$ subarrays supports K users either with or without RISs. The *i*th subarray of the BS is a UPA having $m_{t,i} \times n_{t,i}$ antenna units. For simplicity and without loss of generality, we let $m_{t,i} = m_t$, $n_{t,i} = n_t$, $i = 1, ..., L_B$. Note that L_B is also the number of RF chains, since each BS subarray is controlled by a dedicated RF chain. Due to limited processing power, there is only a single subarray baseband and RF chain consisting of $m_{r,k} \times n_{r,k}$ tightly-packed elements at the *k*th user. For simplicity and without loss of generality, we let $m_{r,k} = m_r$, $n_{r,k} = n_r$, $k = 1, ..., K$. The number L_B of antenna subarrays is assumed to be higher than K for attaining high gains. UPAs are promising for THz communications both in BS and user terminals, since they can accommodate more antenna elements by a two-dimensional subarray for 3D beamforming.

In THz communications, the link from the BS to the user may be blocked. Hence we assume that the line-of-sight (LOS) link from the BS to each user is indeed blocked, and a RIS is applied for improving the link spanning from the BS to the user by reflecting the signal. The RIS consists of a sub-wavelength UPA having Υ passive reflecting elements under the control of an RIS controller. The THz channel is highly frequency-selective, but there are several low-attenuation windows separated by high-attenuation spectral nulls owing to molecular absorption [32]. Therefore, we can adaptively partition the total THz signal bandwidth into numerous sub-bands, say C sub-bands. The *h-th sub-band is centered around the frequency* $f_h, h = 1, 2, \ldots, C$ and it has a width of Π_{f_h}. If Π_h is small enough, the channel can be regarded as frequency-non-selective and the noise power spectral density appears to be locally flat. Thus, for the *h*-th subband signal, we will discuss the direct path spanning from the BS to the user and that from the BS to the user via RIS, i.e. the BS-RIS-UE path.

(1) ***The direct BS-user path***

The received signal of user k can be expressed as

$$\bar{y}_k = \mathbf{v}_k^H \mathbf{Q}_k \mathbf{W} \mathbf{F} \mathbf{s} + \mathbf{v}_k^H \mathbf{n}_k, \ k = 1, ..., \ K, \tag{1}$$

where $\mathbf{s} = [s_1, s_2, ..., s_K]^T$ is a $K \times 1$ vector containing the transmitted symbols of K users, so that $\mathbb{E}\{\mathbf{s}\mathbf{s}^*\} = \frac{P_s}{K}\mathbf{I}_K$, where P_s denotes the total initial transmit power and the same power is assigned to each user. In (1), $\mathbf{Q}_k$ is the $m_r n_r \times L_B m_t n_t$ THz channel matrix between the BS and user k. The LOS components of the direct BS-user links are blocked by obstacles, so we assume that the direct link channel $\mathbf{Q}_k$ contains only *non-line-of-sight* (NLOS) components; $\mathbf{W}$ is the $L_B m_t n_t \times L_B$ analog transmit beamforming matrix representing the equal power splitters and phase shifters. For the array-of-subarray structure of (1), $\mathbf{W}$ is block-diagonal structure and can be expressed as

$$\mathbf{W} = \begin{bmatrix} \mathbf{w}_1 & \mathbf{0} & \cdots & \mathbf{0} \\ \mathbf{0} & \mathbf{w}_2 & \cdots & \mathbf{0} \\ \vdots & \vdots & \vdots & \vdots \\ \mathbf{0} & \mathbf{0} & \cdots & \mathbf{w}_{L_B} \end{bmatrix}, \tag{2}$$

where $\mathbf{w}_l$ is an $m_t n_t \times 1$ vector with $|(\mathbf{w}_l)_a| = \frac{1}{\sqrt{m_t n_t}}$, $l = 1, ..., L_B$, $a = 1, ..., m_t n_t$. Still referring to (1), $\mathbf{F}$ is the $L_B \times$

TABLE I
OUR NOVEL CONTRIBUTIONS CONTRASTED TO THE STATE-OF-THE ART

	our paper	[30]-2015	[11]-2019	[8]-2019	[9]-2019	[13]-2019	[22]-2020	[31]-2021	[3]-2021	[16]-2021	[21]-2021
Joint BS array-of-subarrays and sub-RIS architecture for spatial multiplexing	√										
Near-field and far-field path-loss of RIS-aided THz channels	√										
Sensor-based beam training	√										
Hybrid 3D beamforming	√										
RIS aided systems	√		√	√	√	√	√	√		√	√
THz Communications	√	√		√					√		√
Precise beamforming	√										
multi-user massive MIMO systems	√										√

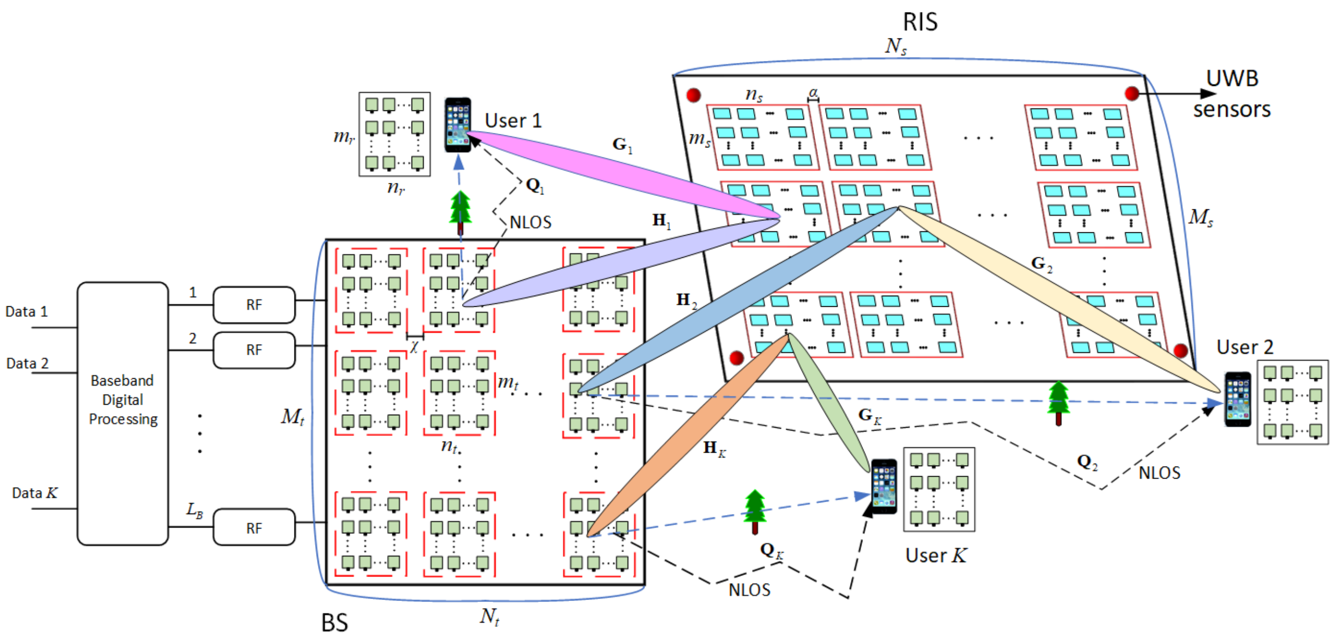

Fig. 1. System model of 3D hybrid beamforming and sensor-based channel estimation for RIS-aided THz multi-user massive MIMO systems.

K baseband digital beamforming matrix used for interference mitigation, where we have

$$\mathbf{F} = [\mathbf{f}_1, \mathbf{f}_2, \dots, \mathbf{f}_K], \quad (3)$$

with

$$||\mathbf{W}\mathbf{f}_k||^2 = 1; \quad (4)$$

$\mathbf{f}_k$ is a $L_B \times 1$ vector of the kth user; $\mathbf{v}_k$ is the $m_r n_r \times 1$ receive analog beamforming vector applied by user k with $|(\mathbf{v}_k)_b| = \frac{1}{\sqrt{m_r n_r}}$, $b = 1, ..., m_r n_r$; $\mathbf{n}_k$ is the $m_r n_r \times 1$ Gaussian noise vector at user k, i.e., $\mathbf{n}_k \sim \mathcal{N}(\mathbf{0}, \sigma_k^2 \mathbf{I})$, $k = 1$,..., K.

(2) ***The RIS-aided path***

The RIS consists of a sub-wavelength UPA having Υ passive reflecting elements. According to the subarray structure of the BS, we also partition the RIS into $L_s = M_s \times N_s$ sub-RISs. The ith sub-RIS consists of $m_{s,i} \times n_{s,i}$ elements, $i = 1, ..., L_s$. Each sub-RIS is the dual counterpart of every subarray of the BS. Thus, we have $\Upsilon = \sum_{i=1}^{L_s} m_{s,i} n_{s,i}$. The adjacent elements are separated by $\varrho \geq \lambda_{spp}$, where λ_{spp} is the *Surface Plasmon Polariton* (SPP) wavelength [3], so the mutual coupling between the elements is neglected. For simplicity and without loss of generality, we let $m_{s,i} = m_s$, $n_{s,i} = n_s$, $i = 1, ..., L_s$.

Let the THz channels spanning from the BS to RIS, and from the RIS to user k, be denoted by $\mathbf{G}$ and $\mathbf{H}_{k,o}$, respectively. The RIS reflection matrix is denoted by $\mathbf{O}$ and the reflection matrix from the kth sub-RIS to user k is denoted by $\mathbf{O}_k$. For the sub-RIS structure, $\mathbf{O}$ is an $L_s m_s n_s \times L_s m_s n_s$ block matrix

$$\mathbf{O} = \left[\begin{array}{cccc} \mathbf{O}_1 & \mathbf{0} & \cdots & \mathbf{0} \\ \mathbf{0} & \mathbf{O}_2 & \cdots & \mathbf{0} \\ \vdots & \vdots & \vdots & \vdots \\ \mathbf{0} & \mathbf{0} & \cdots & \mathbf{O}_{L_s} \end{array} \right], \tag{5}$$

where $\mathbf{O}_k$ is an $m_s n_s \times m_s n_s$ matrix; $\mathbf{O}_k = \mathrm{diag}(\mathbf{q}_k)$, where $\mathbf{q}_k = \left[e^{k\theta_{1,k}}, \ldots, e^{k\theta_{i,k}}, \ldots, e^{k\theta_{m_s n_s,k}}\right]^T$, $\theta_{i,k}$ is the phase of the i-th reflection element in the k-th sub-RIS, $i = 1, ..., m_s n_s$. Without loss of generality, we assume that the number of sub-RISs is $L_s = K$ and the k-th sub-RIS reflects the signals for the k-th user. Thus, we propose a joint hybrid 3D beamforming–BS array-of-subarray and the corresponding sub-RIS architecture. Further details will be given in the following sections.

The received signal of user k can be expressed as

$$\tilde{y}_k = \mathbf{v}_k^H \mathbf{H}_{k,o} \mathbf{OGWFs} + \mathbf{v}_k^H \mathbf{n}_k, \tag{6}$$

where $\mathbf{G}$ is the $L_s m_s n_s \times L_B m_t n_t$ element channel matrix of the line spanning from the BS to the RIS. Furthermore, $\mathbf{H}_{k,o}$ is the $m_r n_r \times L_s m_s n_s$ channel matrix of the line emerging from the RIS to the user *k*. Observe that $\tilde{y}_k$ can also be expressed in the form of the desired and interference terms as follows:

$$\tilde{y}_k = \mathbf{v}_k^H \mathbf{H}_{k,o} \mathbf{OGW} \mathbf{f}_k s_k + \mathbf{v}_k^H \mathbf{H}_{k,o} \mathbf{OG} \sum_{i \neq k}^{K} \mathbf{W} \mathbf{f}_i s_i + \mathbf{v}_k^H \mathbf{n}_k. \tag{7}$$

The RIS-aided THz channel is dominated by the LOS path and some indirect BS-RIS rays of NLOS propagation due to reflections and scattering [30] imposed by the quasi-optical characteristics of THz signals. Let $\mathbf{G}_k$ denote the $m_t n_t \times m_s n_s$ channel matrix of the line spanning from the k-th BS subarray to the k-th sub-RIS, while $\mathbf{H}_k$ denotes the $m_r n_r \times m_s n_s$ channel matrix of the line spanning from the k-th sub-RIS to the k-th user. Thus, $\mathbf{G}_k$ and $\mathbf{H}_k$ are modeled by

$$\begin{aligned} \mathbf{G}_k &= \bar{\mathbf{G}}_k + \tilde{\mathbf{G}}_k \\ &= \sqrt{m_t n_t m_s n_s} [\beta_{1,k}^L \mathbf{a}_{sa,k} \left(\delta_k, \kappa_k\right) \mathbf{a}_{t,k}^H \left(\psi_k, \tau_k\right) \\ &+ \sum_{i=1}^{n_{NL}} \beta_{1,k,i}^{NL} \mathbf{a}_{sa,k,i} \left(\delta_{k,i}^{NL}, \kappa_{k,i}^{NL}\right) \mathbf{a}_{t,k,i}^H \left(\psi_{k,i}^{NL}, \tau_{k,i}^{NL}\right)], \end{aligned} \tag{8}$$

$$\begin{aligned} \mathbf{H}_k &= \bar{\mathbf{H}}_k + \tilde{\mathbf{H}}_k \\ &= \sqrt{m_r n_r m_s n_s} [\beta_{2,k}^L \mathbf{a}_{r,k} \left(\vartheta_k, \phi_k\right) \mathbf{a}_{sd,k}^H \left(\varsigma_k, \varphi_k\right) \\ &+ \sum_{i=1}^{\tilde{n}_{NL}} \beta_{2,k,i}^{NL} \mathbf{a}_{r,k,i} \left(\vartheta_{k,i}^{NL}, \phi_{k,i}^{NL}\right) \mathbf{a}_{sd,k,i}^H \left(\varsigma_{k,i}^{NL}, \varphi_{k,i}^{NL}\right)]. \end{aligned} \tag{9}$$

where $\bar{\mathbf{G}}_k$ and $\bar{\mathbf{H}}_k$ represent the LOS components, while $\tilde{\mathbf{G}}_k$ and $\tilde{\mathbf{H}}_k$ denote the NLOS components; ψ_k ($\psi_{k,i}^{NL}$), τ_k ($\tau_{k,i}^{NL}$) are the azimuth and elevation AODs (*angle of departure*) at the k-th BS subarray, respectively; ϑ_k ($\vartheta_{k,i}^{NL}$), ϕ_k ($\phi_{k,i}^{NL}$) are the azimuth and elevation AOAs (*angle of arrival*) at the k-th user, respectively; δ_k ($\delta_{k,i}^{NL}$), $\kappa_k(\kappa_{k,i}^{NL})$ are the azimuth and elevation AOAs from the k-th BS subarray to the k-th sub-RIS, respectively; $\varsigma_k(\varsigma_{k,i}^{NL})$, φ_k ($\varphi_{k,i}^{NL}$) are the azimuth and elevation AODs from the k-th sub-RIS to the k-th user, respectively; n_{NL} and $\tilde{n}_{NL}$ are the numbers of NLOS components; $\beta_{1,k}^L$ and $\beta_{2,k}^L$ denote the corresponding THz LOS complex gains given by

$$\begin{aligned} |\beta_{g,k}^L|^2 &= \xi_{g,k}^L \left(d_{g,k}, f_h\right) \\ &= \frac{c^2}{\left(4\pi d_{g,k} f_h\right)^2} \exp\left[-\mu\left(f_h\right) d_{g,k}\right], \ g = 1, 2, \end{aligned} \tag{10}$$

where $\xi_{1,k}^L$ and $\xi_{2,k}^L$ are the corresponding THz LOS path-loss, $\mu\left(f_h\right)$ is the absorption coefficient at frequency f_h, $d_{1,k}$ is the distance from the BS to the RIS, $d_{2,k}$ is the distance from the RIS to the user, both for user k, and c is the speed of light. Still referring to (8) and (9), $\beta_{1,k,i}^{NL}$ and $\beta_{2,k,i}^{NL}$ denote the corresponding THz NLOS complex gains.

In Eq. (8) and (9), $\mathbf{a}_{t,k}\left(\psi_k, \tau_k\right)$, and $\mathbf{a}_{r,k}\left(\vartheta_k, \phi_k\right)$ are the antenna array steering vectors at the k-th BS subarray and k-th user, respectively:

$$\begin{aligned} &\mathbf{a}_{t,k}\left(\psi_k, \tau_k\right) \\ &= \frac{1}{\sqrt{m_t n_t}} \Big[1, \ldots, e^{j\frac{2\pi r}{\lambda}\left[x_1 \cos\psi_k \sin\tau_k + y_1 \sin\psi_k \sin\tau_k\right]} \\ &\quad \ldots, e^{j\frac{2\pi r}{\lambda}\left[(m_t-1)\cos\psi_k \sin\tau_k + (n_t-1)\sin\psi_k \sin\tau_k\right]}\Big]^T, \end{aligned} \tag{11}$$

where x_1 and y_1 denote the index of the BS antenna element, $0 < x_1 \leq m_t - 1$, $0 < y_1 \leq n_t - 1$. Additionally, r is the distance between the BS antenna elements, and λ represents the wavelength of THz signals. Still referring to (9), we have

$$\begin{aligned} &\mathbf{a}_{r,k}\left(\vartheta_k, \phi_k\right) \\ &= \frac{1}{\sqrt{m_r n_r}} \Big[1, \ldots, e^{j\frac{2\pi\gamma}{\lambda}\left[x_2 \cos\vartheta_k \sin\phi_k + y_2 \sin\vartheta_k \sin\phi_k\right]} \\ &\quad \ldots, e^{j\frac{2\pi\gamma}{\lambda}\left[(m_r-1)\cos\vartheta_k \sin\phi_k + (n_r-1)\sin\vartheta_k \sin\phi_k\right]}\Big]^T, \end{aligned} \tag{12}$$

where x_2 and y_2 denote the index of the user antenna element, $0 < x_2 \leq m_r - 1$, $0 < y_2 \leq n_r - 1$; and γ is the distance between the user antenna elements.

Explicitly, $\mathbf{a}_{sa,k}(\delta_k, \kappa_k)$ and $\mathbf{a}_{sd,k}(\varsigma_k, \varphi_k)$ in Eq. (8) and (9) are the arrival and departure steering vectors at the k-th sub-RIS, respectively. They can be expressed as follows:

$$\begin{aligned} &\mathbf{a}_{sa,k}(\delta_k, \kappa_k) \\ &= \frac{1}{\sqrt{m_s n_s}} \Big[1, \ldots, e^{j\frac{2\pi\varrho}{\lambda}\left[x_s \cos\delta_k \sin\kappa_k + y_s \sin\delta_k \sin\kappa_k\right]} \\ &\quad \ldots, e^{j\frac{2\pi\varrho}{\lambda}\left[(m_s-1)\cos\delta_k \sin\kappa_k + (n_s-1)\sin\delta_k \sin\kappa_k\right]}\Big]^T, \end{aligned} \tag{13}$$

$$\begin{aligned} &\mathbf{a}_{sd,k}(\varsigma_k, \varphi_k) \\ &= \frac{1}{\sqrt{m_s n_s}} \Big[1, \ldots, e^{j\frac{2\pi\varrho}{\lambda}\left[x_s \cos\varsigma_k \sin\varphi_k + y_s \sin\varsigma_k \sin\varphi_k\right]} \\ &\quad \ldots, e^{j\frac{2\pi\varrho}{\lambda}\left[(m_s-1)\cos\varsigma_k \sin\varphi_k + (n_s-1)\sin\varsigma_k \sin\varphi_k\right]}\Big]^T, \end{aligned} \tag{14}$$

where x_s and y_s denote the index of the RIS element, $0 < x_s \leq m_s - 1$, $0 < y_s \leq n_s - 1$; and ϱ is the distance between the RIS elements within the sub-RIS.

Therefore, upon combining (1) and (6), the signal received by user k from the BS-user and from the BS-RIS-user channels can be expressed as

$$y_k = \bar{y}_k + \tilde{y}_k. \tag{15}$$

The THz channels are sparse and only few paths exists [30]. Moreover, the power difference of the THz signals between the LOS and NLOS path is significant. Specifically, the power of the first-order reflected path is attenuated by more than 10 dB on average compared to the LOS path and that of the second-order reflection by more than 20 dB [30], so THz channels are LOS-dominant and the small-scale fading can be ignored. Thus, we will focus on the LOS path of the THz signal when exploring the channel condition, while relying on a RIS, and on beamforming schemes. Furthermore, considering the beamforming gain of the transceivers and the gains of the RIS, the received power of the BS-user link in (15) is much lower than that of the BS-RIS-user link.

III. Conditions of Spatial Multiplexing for the Proposed Architecture

In this section, we discuss the conditions of achieving high multiplexing gains for the proposed RISs-aided THz architecture. Since the propagation of signals at THz frequencies is "quasi-optical", the LOS path dominates the channel complemented only by a few non-LOS (NLOS) reflected rays due to the associated high reflection loss. Thanks to the beamforming gain and flexible placement of RISs, a LOS path may be present between each pair of the BS subarrays, the sub-RIS and the user's receiver subarrays. To achieve high multiplexing gains in strong LoS environments at high frequencies [3], the antenna spacing of both the TX and RX together with that of the RIS element spacing should be set much larger than the operating THz wavelength.

We first consider the BS-RIS channel. We denote the distances between two adjacent subarrays at the BS transmitter and two adjacent sub-RIS respectively by χ and α. Without loss of generality, we assume symmetry in the remainder of the paper, i.e., $M_t = N_t = M$, $M_s = N_s = N$. Thus, the BS contains $M \times M$ subarrays and the RIS contains $N \times N$ sub-RISs. The capacity is maximized when all columns of $\mathbf{G}$ are orthogonal. According to the duality of the communication transmission, the optimal spacing of the sub-RISs should be the same as the optimal spacing of the BS sub-arrays. Hence we formulate Theorem 1 as follows.

Theorem 1. To achieve spatial multiplexing gain for the BS to the RIS line, the optimal spacing of the sub-RISs or the BS subarrays is

$$\alpha_{op} = \sqrt{q\frac{d_1\lambda}{N}} \tag{16}$$

for integer values of q, where d_1 is the distance from the BS to the RIS, while λ is the wavelength of the THz signal.

Proof. The proof is given in Appendix A.

Theorem 2. To achieve a high spatial multiplexing gain for the RIS to BS uplink, the optimal spacing of the BS subarrays or the sub-RISs is

$$\chi_{op} = \sqrt{q\frac{d_1\lambda}{M}} \tag{17}$$

for integer values of q, where d_1 is the distance between the centers of the RIS and BS arrays, and λ is the wavelength of the THz signal.

Proof. The proof is similar to that of Theorem 1, hence it is omitted here.

Let Ψ denote the minimal common multiple of $\frac{1}{N}$ and $\frac{1}{M}$. Then, after combining the condition (16) and condition (17), we arrive at the unified optimal sub-RIS and BS subarray design condition formulated as follows:

$$\alpha_{op} = \chi_{op} = \sqrt{qd_1\lambda\Psi} \tag{18}$$

for integer values of q, where d_1 is the distance between the centers of the RIS and BS arrays, and λ is the wavelength of the THz signal.

Thus, for the *h*-th subband signal, the unified optimal sub-RIS and BS subarray design condition should satisfy

$$\alpha_{op,h} = \chi_{op,h} = \sqrt{q\frac{d_1c}{f_h}\Psi} \tag{19}$$

The separation of elements in the BS subarrays or sub-RISs may be achieved via spatial interleaving. Moreover, the required spacing can be realized by choosing the right elements belonging to each BS subarray or sub-RIS. Each BS subarray associated with the corresponding sub-RIS may focus on a specific individual subband of the THz signal and can also be tuned flexibly according to the different user distances.

Let us now consider the channels spanning from the sub-RISs to the users. At the receiver side, each user has a subarray and is generally separated, so the distance of two adjacent user subarrays is usually large. Naturally, we cannot impose any constraints on the user positions, which tend to be random. So we must resort to exploiting the frequency selectivity of the THz channels for spatial multiplexing. According to [30], the THz channels have limited angular spread of about $40°$. Since the beam steering vectors associated with completely different angles of large-scale antennas are nearly orthogonal, for the channels spanning from the *i*th and the *k*th sub-RIS to user *k,* we have

$$\mathbf{a}_{sd,i}^H(\varsigma_i,\varphi_i)\mathbf{a}_{sd,k}(\varsigma_k,\varphi_k) \simeq 0, \quad \varsigma_i \neq \varsigma_k, \varphi_i \neq \varphi_k. \tag{20}$$

As the RIS may be regarded as a large-scale antenna array, the channel from the RIS to the user can be nearly orthogonal, hence beneficial spatial multiplexing gains can be achieved. For users that are close enough to be within the angular spread, the pre-scanning and grouping technique of [30] can be adopted.

IV. Path-loss of the RIS-aided Near-Field and Far-Field THz Channel

Based on the assumption that the spherical wave generated by the transmitter can be approximately regarded as a plane wave at the RIS side when a transmitter is far away from the RIS, the far-field and near-field boundary of the antenna array is defined as $D = \frac{2L^2}{\lambda}$, where D, L and λ represent the distance between the transmitter and the center of the antenna array, the maximum dimension of the antenna array and the wavelength of the signal, respectively [31]. For the RIS of the proposed architecture, we have

$$D = \frac{2N^2 m_s n_s d_x d_y}{\lambda}. \tag{21}$$

Generally, $d_x = d_y = \frac{\lambda}{2}$, so we get

$$D = \frac{N^2 m_s n_s \lambda}{2}. \tag{22}$$

Hence, for the hth subband THz signal, we have

$$D_h = \frac{N^2 m_s n_s c}{2 f_h} \tag{23}$$

Let us now discuss the THz channel path-loss in the near-field and far-field of the kth sub-RIS, respectively. Let us represent the kth sub-RIS-aided cascaded channel by

$$\mathbf{Z}_k = \mathbf{H}_k \mathbf{O} \mathbf{G}. \tag{24}$$

Corollary 1. For near-field beamforming over the RIS-aided THz channel, the path-loss of $\mathbf{Z}_k$ of the kth user can be expressed by

$$\zeta_k = \frac{c^2}{(4\pi f)^2 (d_{1,k} + d_{2,k})^2} e^{-\mu(f)(d_{1,k}+d_{2,k})}. \tag{25}$$

where $d_{1,k}$ is the effective distance from the kth BS subarray to the kth sub-RIS, and $d_{2,k}$ is the effective distance from the kth sub-RIS to the kth user.

Proof. Based on the path-loss of the near-field RIS-aided beamforming [31] and the THz channel (10), the path-loss of the cascaded BS-RIS-user channel $\mathbf{Z}_k$ can be formulated as

$$\begin{aligned} \zeta_k &= \xi^L (d_{1,k} + d_{2,k}, f) \\ &= \frac{c^2}{(4\pi f)^2 (d_{1,k} + d_{2,k})^2} e^{-\mu(f)(d_{1,k}+d_{2,k})}. \end{aligned}$$

Explicitly, the signal transmission process is equivalent to that of a signal traveling the distance $d_{1,k} + d_{2,k}$.

Corollary 2. For far-field beamforming over the RIS-aided THz channel, the path-loss of $\mathbf{Z}_k$ of the kth user can be expressed as

$$\hat{\zeta}_k = \frac{c^2}{(4\pi f)^2 d_{1,k}^2 d_{2,k}^2} e^{-\mu(f)(d_{1,k}+d_{2,k})}. \tag{26}$$

where $d_{1,k}$ is the effective distance from the kth BS subarray to the kth sub-RIS, and $d_{2,k}$ is the effective distance from the kth sub-RIS to the kth user.

Proof. According to the path-loss of the far-field RIS-aided beamforming [31] and the THz channel (10), the path-loss of the cascaded BS-RIS-user channel $\mathbf{Z}_k$ can be formulated as

$$\hat{\zeta}_k = \frac{c^2}{(4\pi f)^2 d_{1,k}^2 d_{2,k}^2} e^{-\mu(f)(d_{1,k}+d_{2.k})}.$$

V. Sensor-based Channel Estimation and Beam Training Scheme

In order to realize the proposed joint hybrid 3D beamforming BS array-of-subarray and the corresponding sub-RIS architecture, in this section, we propose a sensor-based channel estimation and beam training scheme. The location information obtained by the sensor allows us to expedite the channel estimation and beamforming processes.

Given the RIS-aided THz channel models of Section II, estimating the RIS-aided channel is equivalent to inferring the parameters of the channel paths; namely the AoA, the AoD, and the path-loss of each path. The RIS locations are generally known by the BS. Four UWB sensors are integrated into the four corners of the RIS, as shown in Fig. 1, which is the minimum number of UWB nodes required for supporting 3D localization. Thanks to the ultra-low power density and 3.1-10.6 GHz frequency band of UWB, the interference between the UWB ranging signal and the THz signals is negligible. The distance between each UWB sensor and the user can be estimated using either a *Time-of-Arrival* (TOA) or *Two-Way Time of-Flight* (TW-ToF) based ranging method [33]. However, they introduce the ranging error ε. Then, the 3D user position can be determined by multi-lateration algorithm upon solving a set of nonlinear equations:

$$[x_{s_i} - x_U]^2 + [y_{s_i} - y_U]^2 + [z_{s_i} - z_U]^2 = \tilde{d}_i^2 \tag{27}$$

where $i = \{1, 2, 3, 4\}$, $P_{s_i} = [x_{s_i}, y_{s_i}, z_{s_i}]$ indicates the coordinates of each UWB node on the RIS, $P_U = [x_U, y_U, z_U]$ is the unknown user position, and $\tilde{d}_i = d_i + \varepsilon = |P_U - P_{s_i}| + \varepsilon$ is the measurement of the distance between the UWB sensors and the UE. Given the ranging error ε, an approximate of (27) must be used instead of the intersection of four spheres at a single point found in the ideal scenario [33].

We then adopt the user location information provided by the UWB sensors to obtain angle and path-loss of the LOS path. The AOD/AOA of the LOS path can be inferred by trigonometry as follows.

Without loss of generality, the k-th BS subarray and the k-th sub-RIS of Fig. 1 are assumed to be located at $(x_{B,k}, y_{B,k}, z_{B,k})$ and $(0, 0, 0)$, respectively. Then the effective AOA at the k-th sub-RIS from the k-th BS subarray can be calculated as

$$\delta_k = \arctan\left(\frac{y_{B,k}}{x_{B,k}}\right), \tag{28}$$

$$\kappa_k = \arcsin\left(\frac{z_{B,k}}{d_{1,k}}\right), \tag{29}$$

where $d_{1,k} = \sqrt{x_{B,k}^2 + y_{B,k}^2 + z_{B,k}^2}$.

Similarly, the effective AOD from the k-th BS subarray to the k-th sub-RIS are:

$$\psi_k = -\delta_k, \tag{30}$$

$$\sigma_k = -\kappa_k. \tag{31}$$

Therefore, according to (11) and (13), $\mathbf{a}_{t,k}(\psi_k, \sigma_k)$ and $\mathbf{a}_{sa,k}(\delta_k, \kappa_k)$ can be obtained.

Let $(\hat{x}_{U,k}, \hat{y}_{U,k}, \hat{z}_{U,k})$ denote the estimated location of user k obtained by the UWB sensors.The k-th sub-RIS calculates its effective AOD from itself to the k-th user as

$$\hat{\varsigma}_k = \arctan\left(\frac{\hat{y}_{U,k}}{\hat{x}_{U,k}}\right), \tag{32}$$

$$\hat{\varphi}_k = \arcsin\left(\frac{\hat{z}_{U,k}}{\hat{d}_{2,k}}\right), \tag{33}$$

where $\hat{d}_{2,k} = \sqrt{\hat{x}_{U,k}^2 + \hat{y}_{U,k}^2 + \hat{z}_{U,k}^2}$.

Similarly, the k-th user calculates its effective AOA from itself to the k-th sub-RIS as

$$\hat{\vartheta}_k = -\hat{\varsigma}_k, \tag{34}$$

$$\hat{\phi}_k = -\hat{\varphi}_k. \tag{35}$$

Thus, according to (14) and (12), $\mathbf{a}_{sd,k}(\hat{\varsigma}_k, \hat{\varphi}_k)$ and $\mathbf{a}_{r,k}\left(\hat{\vartheta}_k, \hat{\phi}_k\right)$ can be obtained. By substituting $d_{1,k}$ and $\hat{d}_{2,k}$ into (25) and (26), we can formulate the channel gain. In fact, these channel gains are almost deterministic due to the LOS-dominant characteristic of the RIS-aided THz channels, hence the small-scale fading can be ignored.

A. Analog Active Beamforming Relying on User Locations

Then, the estimated angle information can be used to design the BS subarray's active beamforming and sub-RIS's passive beamforming. However, because the active and the passive beamforming are coupled, the optimization problem is non-convex, so the global optimum is typically a challenge to find. Although some suboptimal algorithms have been proposed for MISO systems relying on alternating optimization [16], the computational complexity of these algorithms is excessive because of the large number of reflection elements. Hence we circumvent this challenge by opting for the low-complexity separate optimization of the BS subarray and of each sub-RIS, because then convenient closed-form solutions can be obtained. Specifically, the BS utilizes the angle information of the BS-RIS link to design the active beamforming. Without loss of generality, we assume that the k-th user is assisted by the k-th sub-RIS. Thus, the active beamforming designed for the k-th user should be aligned to the k-th sub-RIS. As such, the transmit beam of the k-th BS subarray is designed as

$$\mathbf{w}_k = \sqrt{p_k}\mathbf{a}_{t,k}\left(\psi_k, \sigma_k\right), \tag{36}$$

where p_k is the transmit power of the k-th BS subarray. For the transmit power equally divided among BS subarrays corresponding to different users, we have $p_k=\frac{P_s}{K}$. Therefore, the channel between the BS and RIS can be readily estimated with the aid of the previously calibrated accurate angles, and we would only focus our attention on the estimation of the time-variant RIS-UE channels.

The received beam of the k-th user is given by

$$\hat{\mathbf{v}}_k = \sqrt{m_r n_r}\mathbf{a}_{r,k}\left(\hat{\vartheta}_k, \hat{\phi}_k\right). \tag{37}$$

B. RIS Phase Shift Based Passive Beamforming Relying on User Locations

We then use the estimated angle information of the RIS-user link for the RIS phase shift based passive beamforming design. The k-th user's received signal is maximized with the k-th sub-RIS by optimizing the phase shift beam $\mathbf{O}_k$. The optimization problem can be formulated as:

$$\begin{aligned} &\max_{\mathbf{O}_k} \left|\mathbf{v}_k^H\mathbf{H}_k\mathbf{O}\mathbf{G}\mathbf{W}\mathbf{f}_k\right|^2, \\ &\textit{s.t.} \ \left|[\mathbf{O}_k]_{i,i}\right| = 1, \quad i = 1, \ldots, m_s n_s. \end{aligned} \tag{38}$$

According to $\mathbf{y}^H\mathbf{X}\mathbf{z} = \mathbf{x}^T(\mathbf{y}^* \odot \mathbf{z})$ with $\mathbf{X} = \mathrm{diag}(\mathbf{x})$, we have

$$\begin{aligned} \mathbf{v}_k^H\mathbf{H}_k\mathbf{O}\mathbf{G}\mathbf{W}\mathbf{f}_k &= \mathbf{q}_k^T\left[\left(\mathbf{H}_k^T\mathbf{v}_k^*\right) \odot \mathbf{G}\mathbf{W}\mathbf{f}_k\right] \\ &= \mathbf{q}_k^T\left[\left(\mathbf{H}_k^T\mathbf{v}_k^*\right) \odot \mathbf{a}_{sa,k}\right]\mathbf{a}_{t,k}^H\mathbf{W}\mathbf{f}_k. \end{aligned} \tag{39}$$

Thus, the objective function in (38) becomes

$$\left|\mathbf{q}_k^T\left[\left(\mathbf{H}_k^T\mathbf{v}_k^*\right) \odot \mathbf{a}_{sa,k}\right]\right|^2 \left|\mathbf{a}_{t,k}^H\mathbf{W}\mathbf{f}_k\right|^2. \tag{40}$$

According to (4) and (36), $\left|\mathbf{a}_{t,k}^H\mathbf{W}\mathbf{f}_k\right|^2$ is a constant independent of $\mathbf{q}_k$, so the optimization problem equals to

$$\begin{aligned} &\max_{\mathbf{q}_k^T} \left|\mathbf{q}_k^T\left[\left(\mathbf{H}_k^T\mathbf{v}_k^*\right) \odot \mathbf{a}_{sa,k}\right]\right|^2, \\ &\text{s.t.} \ \left|[\mathbf{q}_k]_i\right| = 1, \quad i = 1, \ldots, m_s n_s. \end{aligned} \tag{41}$$

Hence, the solution of the above optimization problem is

$$\mathbf{q}_k = \frac{1}{\beta_{2,k}^L}\left[\left(\mathbf{H}_k^T\mathbf{v}_k^*\right) \odot \mathbf{a}_{sa,k}\right]^*. \tag{42}$$

Using the estimated angles calculated from the position information obtained by the UWB sensors, we design the RIS-aided phase shiftto formulate the passive beam as

$$\hat{\mathbf{q}}_k = \frac{1}{\hat{\beta}_{2,k}^L}\left[\left(\hat{\hat{H}}_k^T\hat{\mathbf{v}}_k^*\right) \odot \mathbf{a}_{sa,k}\right]^*. \tag{43}$$

where $\hat{\hat{\mathbf{H}}}_k = \sqrt{m_r n_r m_s n_s}\hat{\beta}_{2,k}^L\mathbf{a}_{r,k}\left(\hat{\vartheta}_k, \hat{\phi}_k\right)\mathbf{a}_{sd,k}^H\left(\hat{\varsigma}_k, \hat{\varphi}_k\right)$.

Based on (37) and (43), both the phase shift based beamforming and the UE's receiver beamforming both depend on the angles calculated from the estimated user location information obtained by the UWB sensors, which contains positioning errors. The inevitable positioning errors will result in passive transmit beamforming misalignment with the user, which is further aggravated by the UE's receiver beamforming misalgnment with the RIS' transmit beam. Given the extremely narrow pencil beam characteristics of THz signals, the system's performance will thus be severely degraded.

Without being constrained by the positioning errors of the UWB sensors, we further propose the *Precise Beamforming Algorithm* (PBA) for the joint RIS phase shift based beamforming and for the UE's receiver beamforming design.

C. Precise Beamforming Algorithm for joint RIS Phase Shift and UE Receiver Beamforming

As shown in Fig. 2, we propose the PBA for the improved alignment of the RIS's phase shift based beamforming and the UE's receiver beamforming. The accurate position of the kth UE denoted by $(x_{U,k}, y_{U,k}, z_{U,k})$ can be assumed to be uniformly distributed within a sphere with the radius r_e (for UWB positioning, generally $r_e \leq 0.1$ m) and center $(\hat{x}_{U,k}, \hat{y}_{U,k}, \hat{z}_{U,k})$. The optimal active and passive beamforming derived above (contains positioning errors) are used as the initial input value of the algorithm. Thus the efficiency of the beam training algorithm can be substantially improved.

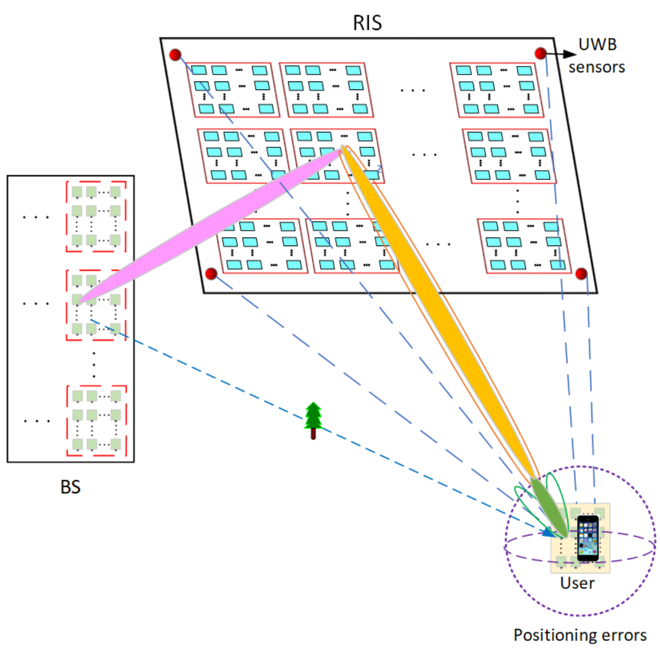

Fig. 2. Precise Beamforming (PBF) for the RIS phase shift beamforming (RIS-BF) and UE receiver beamforming (RBF) design based on the user location.

The algorithm is formulated in Algorithm 1:

It is worth mentioning that the results of optimal beam training may also be fed back to the UWB positioning system for improving its accuracy, which is also a further benefit of joint sensing and communication.

D. Complexity Analysis

In this subsection, we compare the search complexity of our proposed schemes to those of other beam training schemes [21]. The results are shown in Table II. Compared to other schemes, the search time of our proposed scheme is negligible and unrelated to N. By contrast, the complexity of

Algorithm 1 Precise Beamforming Algorithm (PBA) for the RIS-aided phase shift based beamforming (RIS-BF) and UE receiver beamforming (RBF) design

1: Input the RIS phase shift beamforming $\hat{\mathbf{O}}_k$ and the UE RBF $\hat{\mathbf{v}}_k$ obtained above, the receiver beamforming (RBF) codebook $\mathscr{V}$ at the UE and the phase shift based beamforming (RIS-BF) codebook $\mathscr{W}$ at the RIS.
2: For $k = 1 : K$ **do**
3: According to $\hat{\mathbf{v}}_k$ and the range of the UWB positioning errors, select the sub-codebook from $\mathscr{V}$ to obtain $\widetilde{\mathscr{V}_k}$.
4: According to $\hat{\mathbf{O}}_k$ and the range of the UWB positioning errors, select the sub-codebook from $\mathscr{W}$ to obtain $\widetilde{\mathscr{W}_k}$.
5: Search $\widetilde{\mathscr{V}_k}$ to find the optimal RBF $\mathbf{v}_k$ for the kth UE so that $\mathbf{v}_k = argmax \left|\mathbf{v}_k^H \mathbf{H}_k\right|^2$.
6: Search $\widetilde{\mathscr{W}_k}$ to find the optimal RIS-BF $\mathbf{O}_k$ for the kth sub-RIS so that $\mathbf{O}_k = argmax \left|\mathbf{v}_k^H \mathbf{H}_k \mathbf{O}_k\right|^2$.
7: end for
8: Output: $\mathbf{O}_k$ and $\mathbf{v}_k$, $k = 1, 2, ..., K$.

the benchmarks increases. Therefore, the proposed scheme is eminently suitable for time-varying user positions or delay-sensitive applications.

E. Design of the BS's Digital Precoder

Following the beam training and channel estimation using sensor based PBA, we will now design the digital *transmit precoder* (TPC) for interference cancellation among different users. The digital TPC can be designed as follows. Let

$$\mathbf{T}_k = \mathbf{v}_k^H \mathbf{H}_k \mathbf{OGW}. \tag{44}$$

Specifically, the *minimum mean squared error* (MMSE) TPC is formulated as

$$\mathbf{F} = [\mathbf{f}_1, \mathbf{f}_2, \ldots, \mathbf{f}_K] = \left[\left(\mathbf{T}^H\mathbf{T} + \frac{K\sigma^2}{P_s}\mathbf{W}^H\mathbf{W}\right)^{-1}\mathbf{T}^H\right]^{-1}. \tag{45}$$

The *Zero-forcing* (ZF) digital TPC employed as a benchmark is formulated as:

$$\mathbf{F} = [\mathbf{f}_1, \mathbf{f}_2, \ldots, \mathbf{f}_K] = \mathbf{T}^H\left(\mathbf{T}\mathbf{T}^H\right)^{-1}\Delta, \tag{46}$$

where Δ is a diagonal matrix representing the digital TPC power so that $\|\mathbf{Wf}_k\|^2 = 1, k \in \mathcal{K}$. Particularly, the k-th diagonal element of Δ is given by $\Delta_{k,k} = \frac{1}{\|\mathbf{Wf}_k\|}$.

VI. Performance Analysis

Based on the received signal (15), in this section, we characterize the system performance in terms of the achievable sum-rate of the users expressed by

$$R = \mathbb{E}\left\{ [k = 1]K \sum r_k \right\}, \tag{47}$$

where we have:

TABLE II
COMPARISON OF BEAM TRAINING SCHEMES

Beam training schemes	Applicable to RIS-aided system	Applicable to THz	Search time for RIS-aided system
Exhaustive search	Yes	Yes	$N^2 + N^4$
One-side search [34]	No	No	–
Adaptive binary-tree search [35]	No	No	–
Two-stage training scheme [36]	No	Yes	–
Tree dictionary (TD) and PS deactivation (PSD) codebook based search [21]	Yes	Yes	$18N + 12\log_3 N - 3$ (TD) or $6N + 4\log_3 N - 1$ (PSD)
Proposed sensor-based scheme with PBA	Yes	Yes	Negligible and not related to N

$$r_k = \log_2\left(1 + \frac{\frac{P}{K}\left|\mathbf{v}_k^H \mathbf{H}_k \mathbf{OGWf}_k\right|^2}{\frac{P}{K}\sum_{i\neq k}^{K}\left|\mathbf{v}_k^H \mathbf{H}_k \mathbf{OGWf}_i\right|^2 + \left|\mathbf{v}_k^H \mathbf{n}_k\right|^2}\right). \tag{48}$$

According to the orthogonality of different users arranged by the sub-RIS and subarray of the BS, which is achieved by the conditions shown in Section III, as well as the previous digital TPC, we have

$$\frac{P}{K}\sum_{i\neq k}^{K}\left|\mathbf{v}_k^H \mathbf{H}_k \mathbf{OGWf}_i\right|^2 \approx 0. \tag{49}$$

Thus, we arrive at:

$$r_k = \log_2\left(1 + \frac{\frac{P}{K}\left|\mathbf{v}_k^H \mathbf{H}_k \mathbf{OGWf}_k\right|^2}{\left|\mathbf{v}_k^H \mathbf{n}_k\right|^2}\right). \tag{50}$$

Therefore, the performance of the proposed system will not be constrained by the number of users and there is almost no interference among multiple users. As the operation of the system can be carried out in parallel, the algorithm complexity will not be affected by the number of users. In addition, the BS subarrays and sub-RISs can be flexibly configured to meet the needs of different users.

VII. SIMULATION RESULTS AND DISCUSSIONS

In this section, we evaluate the performance of our proposed system architecture and sensor-based channel estimation scheme for RIS-aided THz multi-user massive MIMO systems. We consider both the near-field and far-field of RIS-BF. Since the proposed scheme is capable of accommodating any number of users, it is assumed that there are 4 users having different positions in the simulations. At the BS, each RF chain is connected to a single sub-arrray and each subarray corresponds to a user. Since there is a low-attenuation THz transmission window at 350 GHz [32], we consider the THz frequency subband at 350 GHz in the simulations. The number of channels between the user and the BS is set to 3 due to the sparsity of the THz channels [30]. The simulation parameters are shown in Table III. The user locations are generated randomly and the channel conditions of (20) are satisfied. For the system operating without RISs, the *channel state information* (CSI) is assumed to be perfectly estimated by the BS. For the RIS-aided system, the BS initially does not know the CSI and the channel estimation is conducted based on our proposed scheme. The simulations are conducted in Matlab and 100,000 random runs are performed.

TABLE III
SIMULATION PARAMETERS

Parameters	Symbols	Values	Units
Center frequency of the subband	f_1	350	GHz
Noise power	N_0	–75	dBm
Bandwidth	W	1	GHz
Number of Users	K	4	
Location of the center of the RIS		(0, 0, 0)	m
Location of the center of the BS in the nearfield case		(-0.6, -0.7, 0.4)	m
Locations of the users in the nearfield case		(0, 0, 1.1), (0, 0.45, 0.22), (0.742, 0, 0.3), (0.71, 0.7, 0.1)	m
Location of the center of the BS in the farfield case		(-4, -4, -2)	m
Locations of the users in the farfield case		(2, 2, 1), (0, 3.4, 0.85), (4, 0, 2.07), (0, 0, 5.8)	m

For the far-field scenario, we first assume that each BS antenna subarray is a 4×4 UPA and each user is equipped with one RF chain associated with a 4×4 UPA subarray. Each sub-RIS is also a 4×4 UPA. According to (22), we have $D \approx 0.027$ m. Then we increase the BS antenna subarray, RIS subarray and user subarray to 8×8 UPA and 16×16 UPA. The boundary is $D \approx 0.11$ m and $D \approx 0.44$ m, correspondingly. Therefore, as both the BS and users are in the far-field of the RIS, the locations of the center of the BS arrays and of the RIS are generated randomly, and shown in Table III. For the RIS-aided channel, the distance between the BS and the RIS is 6 m while the distances between the RIS and the users are 3 m, 4.5 m, 3.5 m and 5.8 m, respectively. The simulation results are shown in Fig. 3 (a)-(c). Observe that without the proposed sensor based beam training and channel estimation the performance of RIS-aided channel associated with random phase is only a little better than that without the RIS. For comparison, our proposed scheme achieves much higher spectral efficiency than the original system operating without the RIS, since our system architecture can effectively exploit the spatial multiplexing gain of the RIS-aided THz multi-user massive MIMO systems. Moreover, the sensor based PBA scheme achieves higher spectral efficiency than that without it, because the PBA further eliminates the effect of sensor positioning errors. Compared to the scheme operating without

PBA, our proposed scheme increases the spectral efficiency on average by 10.41%, 10.17%, and 5.19% for the three farfield configurations, respectively. Additionally, the proposed MMSE scheme outperforms its ZF counterpart since ZF may cause noise amplification. Thus, we only characterize the proposed MMSE-based scheme in the following simulations.

For the near-field scenario, each sub-RIS is a 32×32 UPA. According to (22), the boundary is $D \approx 1.76$ m. Then we increase the dimensions of the BS subarray and user subarray from 4×4 UPA to 8×8 UPA. Since both the BS and users are in the near-field of RIS, the locations of the center of the BS and the RIS are generated randomly and are also shown in Table III. The distance between the BS and the RIS is 1 m, while the distances between the RIS and the users are 1 m, 0.5 m, 1.1 m and 0.8 m, respectively. The simulation results are shown in Fig. 4 (a) and (b). Observe that our proposed scheme can also achieve much higher spectral efficiency than the original system operating without RIS. The spectral efficiency of the sensor-based PBA scheme is on average 5.05% and 3.95% higher than that of the scheme operating without PBA, for the two nearfield configurations, respectively. Furthermore, the spectral efficiency in the near-field scenario is much higher than in the far-field scenario, as the path-loss is more severe in the far-field case, which indicates that for better system performance, we can use more RIS elements to create near-field communication for the THz signals.

VIII. Conclusions

A novel joint hybrid 3D beamforming architecture and sensor-based training scheme was proposed for RIS-aided THz multi-user massive MIMO systems. The initially derived optimal active and passive beamformers are employed for RIS-BF and user RBF. A PBA is also proposed for improving the beam alignment accuracy. Compared to the benchmarks, our proposed scheme has lower complexity and search time. We have also derived the conditions of channel orthogonality for the proposed joint architecture to achieve high-integrity spatial multiplexing. Moreover, the closed-form expressions of the near-field and far-field path-loss of the RIS-aided THz channel are derived. Our simulation results show that the spectral efficiency of our proposed system is much higher than that of its counterpart operating without RIS or using a RIS having random phases. Both the near-field and far-field scenarios demonstrate the benefits of our proposed scheme. Our proposed 3D beamforming architecture relying on UPAs has practical potential for emerging RIS-aided THz applications such as integrated networks of terrestrial links, UAVs, and satellite systems. The beamforming optimization feedback would also be beneficial for 3D sensor networks. As our future work, other forms of ISAC will be explored for RIS-aided THz multi-user massive MIMO systems.

IX. Appendix A
Proof of Theorem 1

Proof. Let (x, y) and $(\hat{x}, \hat{y})$ be the coordinates of two arbitrary BS transmit subarrays and (u, v) be arbitrary coordinates

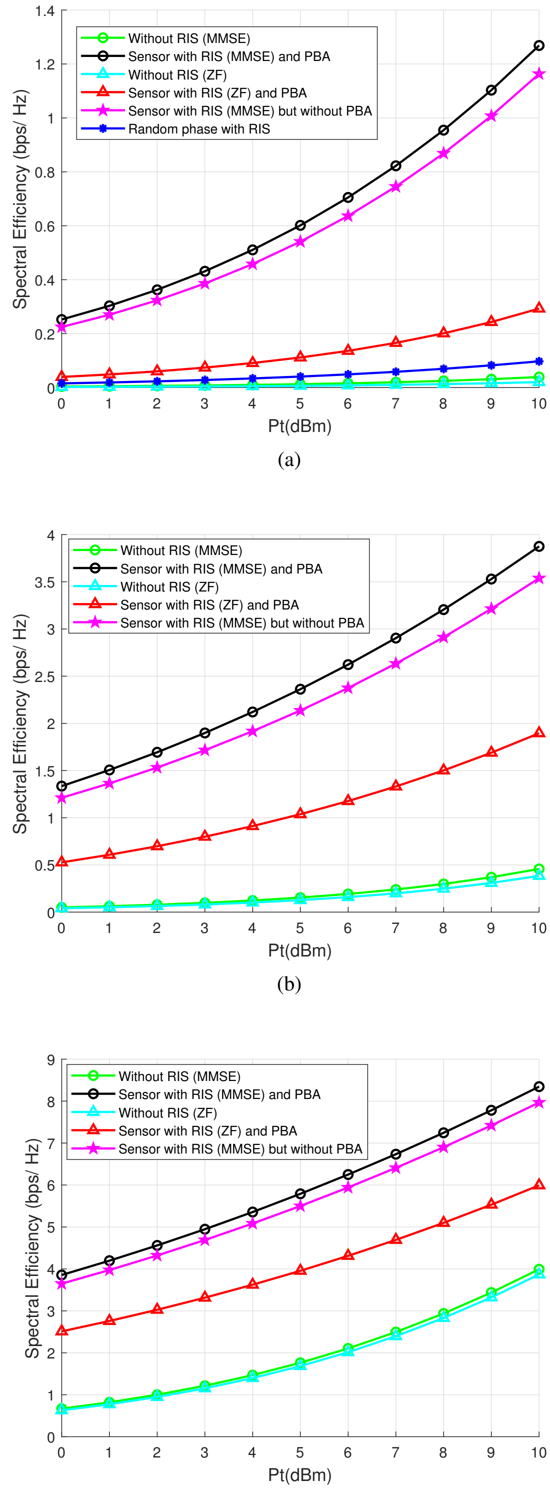

(a) (b) (c)

Fig. 3. Achievable rate (bps/Hz) versus transmit power (dBm) in Far-field case with 4 BS UPA subarrays, 4 UPA sub-RISs and 4 users: (a) BS subarray $\mathbf{4} \times \mathbf{4}$, sub-RIS $\mathbf{4} \times \mathbf{4}$, user UPA $\mathbf{4} \times \mathbf{4}$; (b) BS subarray $\mathbf{8} \times \mathbf{8}$, sub-RIS $\mathbf{8} \times \mathbf{8}$, user UPA $\mathbf{8} \times \mathbf{8}$; (c) BS subarray $\mathbf{16} \times \mathbf{16}$, sub-RIS $\mathbf{16} \times \mathbf{16}$, user UPA $\mathbf{16} \times \mathbf{16}$.

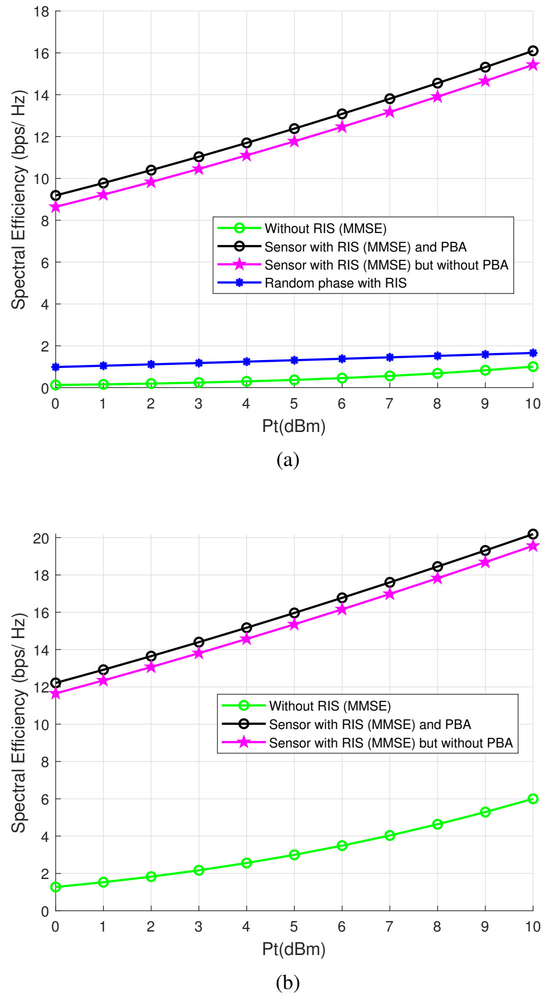

Fig. 4. Achievable rate (bps/Hz) versus transmit power (dBm) in Near-field case with 4 BS UPA subarrays, 4 UPA sub-RISs and 4 users: (a) BS subarray $\mathbf{4} \times \mathbf{4}$, sub-RIS $\mathbf{32} \times \mathbf{32}$, user UPA $\mathbf{4} \times \mathbf{4}$; (b) BS subarray $\mathbf{8} \times \mathbf{8}$, sub-RIS $\mathbf{32} \times \mathbf{32}$, user UPA $\mathbf{8} \times \mathbf{8}$.

of a sub-RIS. The effective distance from the centers of the BS subarray (x, y) and the sub-RIS (u, v) is

$$d_e = \sqrt{d_1^2 + \alpha^2 \left[(u-x)^2 + (v-y)^2 \right]}. \tag{51}$$

For $d_1 \gg \alpha$, according to the binomial approximation, we have

$$d_e \approx d_1 + \frac{\alpha^2 \left[(u-x)^2 + (v-y)^2 \right]}{2d_1}. \tag{52}$$

So we can readily derive the inner product between the corresponding channel columns as

$$\begin{aligned}
&\langle \mathbf{G}_{x,y}, \mathbf{G}_{\hat{x},\hat{y}} \rangle \\
&= \left(\frac{c}{4\pi f d_1} \right)^2 e^{-\mu(f) d_1} \\
&\times \sum_{u=0}^{N-1} \sum_{v=0}^{N-1} e^{k \frac{\pi f}{c d_1} \alpha^2 \left[(u-x)^2 + (v-y)^2 - (u-\hat{x})^2 - (v-\hat{y})^2 \right]} \\
&\cdot \mathbf{a}_{sa,x,y} \left(\delta_{x,y}, \kappa_{x,y} \right) \mathbf{a}_{t,x,y}^H \left(\psi_{x,y}, \sigma_{x,y} \right) \\
&\cdot \mathbf{a}_{sa,k} \left(\delta_{\hat{x},\hat{y}}, \kappa_{\hat{x},\hat{y}} \right) \mathbf{a}_{t,\hat{x},\hat{y}}^H \left(\psi_{\hat{x},\hat{y}}, \sigma_{\hat{x},\hat{y}} \right) \\
&= \left(\frac{c}{4\pi f d_1} \right)^2 e^{-\mu(f) d_1} \\
&\times \sum_{u=0}^{N-1} e^{k \frac{2\pi f}{c d_1} \alpha^2 u (\hat{x}-x)} \sum_{v=0}^{N-1} e^{k \frac{2\pi f}{c d_1} \alpha^2 v (\hat{y}-y)} \\
&\cdot \mathbf{a}_{sa,x,y} \left(\delta_{x,y}, \kappa_{x,y} \right) \mathbf{a}_{t,x,y}^H \left(\psi_{x,y}, \sigma_{x,y} \right) \\
&\cdot \mathbf{a}_{sa,k} \left(\delta_{\hat{x},\hat{y}}, \kappa_{\hat{x},\hat{y}} \right) \mathbf{a}_{t,\hat{x},\hat{y}}^H \left(\psi_{\hat{x},\hat{y}}, \sigma_{\hat{x},\hat{y}} \right).
\end{aligned} \tag{53}$$

The channels are orthogonal when $\langle \mathbf{G}_{x,y}, \mathbf{G}_{\hat{x},\hat{y}} \rangle = 0$. Therefore, without imposing any restrictions on the steering vectors, we can obtain the following optimal value,

$$\alpha_{op} = \sqrt{q \frac{d_1 c}{N f}} = \sqrt{q \frac{d_1 \lambda}{N}} \tag{54}$$

for integer values of q.

References

[1] H. Elayan, O. Amin, B. Shihada, R. M. Shubair, and M.-S. Alouini, "Terahertz Band: The Last Piece of RF Spectrum Puzzle for Communication Systems," *IEEE Open J. Commun. Soc.*, vol. 1, pp. 1–32, 2020. [Online]. Available: https://ieeexplore.ieee.org/document/8901159/

[2] I. F. Akyildiz and J. M. Jornet, "Realizing Ultra-Massive MIMO (1024*1024) communication in the (0.06-10) Terahertz band," *Nano Communication Networks*, vol. 8, pp. 46–54, Jun. 2016. [Online]. Available: https://linkinghub.elsevier.com/retrieve/pii/S1878778916000107

[3] H. Sarieddeen, M.-S. Alouini, and T. Y. Al-Naffouri, "Terahertz-Band Ultra-Massive Spatial Modulation MIMO," *IEEE J. Select. Areas Commun.*, vol. 37, no. 9, pp. 2040–2052, Sep. 2019. [Online]. Available: https://ieeexplore.ieee.org/document/8765243/

[4] C. Lin and G. Y. Li, "Energy-Efficient Design of Indoor mmWave and Sub-THz Systems with Antenna Arrays," *IEEE Trans. Wireless Commun.*, pp. 1–1, 2016. [Online]. Available: http://ieeexplore.ieee.org/document/7436794/

[5] X.-W. Yao, C.-C. Wang, W.-L. Wang, and J. M. Jornet, "On the Achievable Throughput of Energy-Harvesting Nanonetworks in the Terahertz Band," *IEEE Sensors J.*, vol. 18, no. 2, pp. 902–912, Jan. 2018. [Online]. Available: http://ieeexplore.ieee.org/document/8116883/

[6] X. Wang, P. Wang, M. Ding, Z. Lin, F. Lin, B. Vucetic, and L. Hanzo, "Performance Analysis of Terahertz Unmanned Aerial Vehicular Networks," *IEEE Trans. Veh. Technol.*, vol. 69, no. 12, pp. 16 330–16 335, Dec. 2020. [Online]. Available: https://ieeexplore.ieee.org/document/9248588/

[7] A. S. Saadeldin, M. F. O. Hameed, E. M. A. Elkaramany, and S. S. A. Obayya, "Highly Sensitive Terahertz Metamaterial Sensor," *IEEE Sensors J.*, vol. 19, no. 18, pp. 7993–7999, Sep. 2019. [Online]. Available: https://ieeexplore.ieee.org/document/8720258/

[8] X. Ma, Z. Chen, W. Chen, Z. Li, Y. Chi, C. Han, and S. Li, "Joint Channel Estimation and Data Rate Maximization for Intelligent Reflecting Surface Assisted Terahertz MIMO Communication Systems," *IEEE Access*, vol. 8, pp. 99 565–99 581, 2020. [Online]. Available: https://ieeexplore.ieee.org/document/9091552/

[9] C. Pan, H. Ren, K. Wang, M. Elkashlan, A. Nallanathan, J. Wang, and L. Hanzo, "Intelligent Reflecting Surface Aided MIMO Broadcasting for Simultaneous Wireless Information and Power Transfer," *IEEE J. Select. Areas Commun.*, vol. 38, no. 8, pp. 1719–1734, Aug. 2020. [Online]. Available: https://ieeexplore.ieee.org/document/9110849/

[10] C. Pan, H. Ren, K. Wang, J. F. Kolb, M. Elkashlan, M. Chen, M. Di Renzo, Y. Hao, J. Wang, A. L. Swindlehurst, X. You, and L. Hanzo, "Reconfigurable Intelligent Surfaces for 6G Systems: Principles, Applications, and Research Directions," *IEEE Commun. Mag.*, vol. 59, no. 6, pp. 14–20, Jun. 2021. [Online]. Available: https://ieeexplore.ieee.org/document/9475160/

[11] Q. Wu and R. Zhang, "Intelligent Reflecting Surface Enhanced Wireless Network via Joint Active and Passive Beamforming," *IEEE Trans. Wireless Commun.*, vol. 18, no. 11, pp. 5394–5409, Nov. 2019. [Online]. Available: https://ieeexplore.ieee.org/document/8811733/

[12] M. Di Renzo, A. Zappone, M. Debbah, M.-S. Alouini, C. Yuen, J. de Rosny, and S. Tretyakov, "Smart Radio Environments Empowered by Reconfigurable Intelligent Surfaces: How It Works, State of Research, and The Road Ahead," *IEEE J. Select. Areas Commun.*, vol. 38, no. 11, pp. 2450–2525, Nov. 2020. [Online]. Available: https://ieeexplore.ieee.org/document/9140329/

[13] S. Zhang and R. Zhang, "Capacity Characterization for Intelligent Reflecting Surface Aided MIMO Communication," *IEEE J. Select. Areas Commun.*, vol. 38, no. 8, pp. 1823–1838, Aug. 2020. [Online]. Available: https://ieeexplore.ieee.org/document/9110912/

[14] J. Ye, S. Guo, and M.-S. Alouini, "Joint Reflecting and Precoding Designs for SER Minimization in Reconfigurable Intelligent Surfaces Assisted MIMO Systems," *IEEE Trans. Wireless Commun.*, vol. 19, no. 8, pp. 5561–5574, Aug. 2020. [Online]. Available: https://ieeexplore.ieee.org/document/9097454/

[15] Y. Hu, P. Wang, Z. Lin, and M. Ding, "Performance analysis of reconfigurable intelligent surface assisted wireless system with low-density parity-check code," *IEEE Communications Letters*, vol. 25, no. 9, pp. 2879–2883, Sep. 2021.

[16] H. Guo, Y.-C. Liang, J. Chen, and E. G. Larsson, "Weighted Sum-Rate Maximization for Reconfigurable Intelligent Surface Aided Wireless Networks," *IEEE Trans. Wireless Commun.*, vol. 19, no. 5, pp. 3064–3076, May 2020. [Online]. Available: https://ieeexplore.ieee.org/document/8982186/

[17] X. Wei, D. Shen, and L. Dai, "Channel Estimation for RIS Assisted Wireless Communications-Part I: Fundamentals, Solutions, and Future Opportunities," *IEEE Commun. Lett.*, vol. 25, no. 5, pp. 1398–1402, May 2021. [Online]. Available: https://ieeexplore.ieee.org/document/9328501/

[18] A. M. Elbir, A. Papazafeiropoulos, P. Kourtessis, and S. Chatzinotas, "Deep Channel Learning for Large Intelligent Surfaces Aided mm-Wave Massive MIMO Systems," *IEEE Wireless Commun. Lett.*, vol. 9, no. 9, pp. 1447–1451, Sep. 2020. [Online]. Available: https://ieeexplore.ieee.org/document/9090876/

[19] S. Shaham, M. Ding, M. Kokshoorn, Z. Lin, S. Dang, and R. Abbas, "Fast channel estimation and beam tracking for millimeter wave vehicular communications," *IEEE Access*, vol. 7, pp. 141 104–141 118, 2019.

[20] S. Liu, Z. Gao, J. Zhang, M. D. Renzo, and M.-S. Alouini, "Deep Denoising Neural Network Assisted Compressive Channel Estimation for mmWave Intelligent Reflecting Surfaces," *IEEE Trans. Veh. Technol.*, vol. 69, no. 8, pp. 9223–9228, Aug. 2020. [Online]. Available: https://ieeexplore.ieee.org/document/9127834/

[21] B. Ning, Z. Chen, W. Chen, Y. Du, and J. Fang, "Terahertz Multi-User Massive MIMO With Intelligent Reflecting Surface: Beam Training and Hybrid Beamforming," *IEEE Trans. Veh. Technol.*, vol. 70, no. 2, pp. 1376–1393, Feb. 2021. [Online]. Available: https://ieeexplore.ieee.org/document/9325920/

[22] X. Hu, C. Zhong, Y. Zhang, X. Chen, and Z. Zhang, "Location Information Aided Multiple Intelligent Reflecting Surface Systems," *IEEE Trans. Commun.*, vol. 68, no. 12, pp. 7948–7962, Dec. 2020. [Online]. Available: https://ieeexplore.ieee.org/document/9181610/

[23] S. Sharma, A. Gupta, and V. Bhatia, "IR-UWB Sensor Network Using Massive MIMO Decision Fusion: Design and Performance Analysis," *IEEE Sensors J.*, vol. 18, no. 15, pp. 6290–6302, Aug. 2018. [Online]. Available: https://ieeexplore.ieee.org/document/8374926/

[24] F. Liu, C. Masouros, A. P. Petropulu, H. Griffiths, and L. Hanzo, "Joint Radar and Communication Design: Applications, State-of-the-Art, and the Road Ahead," *IEEE Trans. Commun.*, vol. 68, no. 6, pp. 3834–3862, Jun. 2020. [Online]. Available: https://ieeexplore.ieee.org/document/8999605/

[25] F. Liu, C. Masouros, A. Li, H. Sun, and L. Hanzo, "MU-MIMO Communications With MIMO Radar: From Co-Existence to Joint Transmission," *IEEE Trans. Wireless Commun.*, vol. 17, no. 4, pp. 2755–2770, Apr. 2018. [Online]. Available: https://ieeexplore.ieee.org/document/8288677/

[26] J. B. Sanson, D. Castanheira, A. Gameiro, and P. P. Monteiro, "Cooperative Method for Distributed Target Tracking for OFDM Radar With Fusion of Radar and Communication Information," *IEEE Sensors J.*, vol. 21, no. 14, pp. 15 584–15 597, Jul. 2021. [Online]. Available: https://ieeexplore.ieee.org/document/9239392/

[27] M. Jahanbakht, W. Xiang, L. Hanzo, and M. Rahimi Azghadi, "Internet of Underwater Things and Big Marine Data Analytics-A Comprehensive Survey," *IEEE Commun. Surv. Tutorials*, vol. 23, no. 2, pp. 904–956, 2021. [Online]. Available: https://ieeexplore.ieee.org/document/9328873/

[28] J. Liu, Y. Shi, Z. M. Fadlullah, and N. Kato, "Space-Air-Ground Integrated Network: A Survey," *IEEE Commun. Surv. Tutorials*, vol. 20, no. 4, pp. 2714–2741, 2018. [Online]. Available: https://ieeexplore.ieee.org/document/8368236/

[29] A. Singh, M. Andrello, E. Einarsson, N. Thawdarl, and J. M. Jornet, "A Hybrid Intelligent Reflecting Surface with Graphene-based Control Elements for THz Communications," in *2020 IEEE 21st International Workshop on Signal Processing Advances in Wireless Communications (SPAWC)*. Atlanta, GA, USA: IEEE, May 2020, pp. 1–5. [Online]. Available: https://ieeexplore.ieee.org/document/9154305/

[30] C. Lin and G. Y. Li, "Adaptive Beamforming With Resource Allocation for Distance-Aware Multi-User Indoor Terahertz Communications," *IEEE Trans. Commun.*, vol. 63, no. 8, pp. 2985–2995, Aug. 2015. [Online]. Available: http://ieeexplore.ieee.org/document/7116524/

[31] W. Tang, M. Z. Chen, X. Chen, J. Y. Dai, Y. Han, M. Di Renzo, Y. Zeng, S. Jin, Q. Cheng, and T. J. Cui, "Wireless Communications With Reconfigurable Intelligent Surface: Path Loss Modeling and Experimental Measurement," *IEEE Trans. Wireless Commun.*, vol. 20, no. 1, pp. 421–439, Jan. 2021. [Online]. Available: https://ieeexplore.ieee.org/document/9206044/

[32] A. Moldovan, M. A. Ruder, I. F. Akyildiz, and W. H. Gerstacker, "LOS and NLOS channel modeling for terahertz wireless communication with scattered rays," in *2014 IEEE Globecom Workshops (GC Wkshps)*. Austin, TX, USA: IEEE, Dec. 2014, pp. 388–392. [Online]. Available: http://ieeexplore.ieee.org/document/7063462/

[33] F. Lazzari, A. Buffi, P. Nepa, and S. Lazzari, "Numerical Investigation of an UWB Localization Technique for Unmanned Aerial Vehicles in Outdoor Scenarios," *IEEE Sensors J.*, vol. 17, no. 9, pp. 2896–2903, May 2017. [Online]. Available: http://ieeexplore.ieee.org/document/7882672/

[34] T. Nitsche, C. Cordeiro, A. Flores, E. Knightly, E. Perahia, and J. Widmer, "IEEE 802.11ad: directional 60 GHz communication for multi-Gigabit-per-second Wi-Fi [Invited Paper]," *IEEE Commun. Mag.*, vol. 52, no. 12, pp. 132–141, Dec. 2014. [Online]. Available: http://ieeexplore.ieee.org/document/6979964/

[35] A. Alkhateeb, O. El Ayach, G. Leus, and R. W. Heath, "Channel Estimation and Hybrid Precoding for Millimeter Wave Cellular Systems," *IEEE J. Sel. Top. Signal Process.*, vol. 8, no. 5, pp. 831–846, Oct. 2014. [Online]. Available: https://ieeexplore.ieee.org/document/6847111/

[36] C. Lin, G. Y. Li, and L. Wang, "Subarray-Based Coordinated Beamforming Training for mmWave and Sub-THz Communications," *IEEE J. Select. Areas Commun.*, vol. 35, no. 9, pp. 2115–2126, Sep. 2017. [Online]. Available: http://ieeexplore.ieee.org/document/7959180/